http://doi.org/10.29227/IM-2021-02-03 Received: 15 Jul 2021, Accepted: 1 Sep 2021, Published: 10 Nov 2021

Applying Electrical Impedance Tomography Techniques for Detection of Decay Inside Trees

KIEU Duy Thong[1, *], VU Hong Duong[1], NGUYEN Thi Thu Hang[1], NGUYEN Thu Thuy[1]

[1] Hanoi University of Mining and Geology, 18 Vien street, Hanoi, Vietnam

Corresponding author: kieuduythong@humg.edu.vn

Abstract. Trees play a critical role in creating green spaces in public areas such as streets, parks, schools, offices. Over time, the trees often get pests and diseases, and then rotten trees can break. To care for and conserve the trees, it is necessary to determine the condition inside the trunk, especially the possibility of having a hollow or not. Wood decay, modifications of moisture and ion content, density due to biotic and abiotic stress agents of water extremity, salinity, and infection strongly change (di-) electrical properties of wood. Hence, we propose to use electrical impedance tomography to detect the change in electrical properties inside the trees that can link to wood decay. In electrical impedance tomography, an array of electrodes is attached around the tree trunk, and small alternating currents are injected via these electrodes, so the resulting voltages are measured. Processing the data, we can construct the spatial distribution of impedance (or resistivity) of the object. In this work, we will present the preliminary results of our group research. We will show theoretical forward modeling results, followed by laboratory experiments and real data application. The results illustrate that electrical impedance tomography can be useful to define several decay scenarios inside the trees.

Keywords: Electrical impedance tomography, Tree investigation, Resistivity, Conductivity

1. Introduction

Trees play a very important role in creating green space in public areas such as streets, parks, schools, and offices. Over time, trees often suffer from pests and diseases, becoming fragile and susceptible to falling and causing accidents, especially in the rainy season. Thus, determine the tree trunks inside the condition to suggest a suitable treatment plan and minimize damage while keeping the tree intact. In addition, trees are also an important part of historical, cultural, and spiritual works. From 2010 to now, the Vietnam Association for Conservation of Environment and Nature has recognized over 4,000 heritage trees across the country [1]. Since these are perennial plants, a high possibility of having rotten cores inside hollow can occur. A follow-up process is therefore required to care for and preserve these trees. Like people, doctors need X-ray, CT, or nuclear magnetic resonance images to make decisions before treating or operating on patients. Accordingly, we need to have the information of their trunk inside to evaluate the possibility of the trunk being rotten or not. Therefore, it is necessary to apply geophysical techniques to research the tree trunks. The geophysical methods based on electrical properties of the medium such as geoelectrical, electrical resistivity tomography, and electrical impedance tomography are the most used.

The geoelectrical method has been intensively researched and developed both in instruments and data processing [2-4]. This method is very effectively applied in geology, hydrogeology, and engineering [5-7], the study of natural disasters such as landslides [8], research serving agriculture, research branches related to soil [9]. Similarly, electrical tomography has been researched, developed, and applied in many different fields, such as medicine [10, 11] or plant research [12-16].

Techniques similar to impedance tomography have been widely studied and applied in medical imaging [10, 11, 17] and tree investigation [12, 13, 16, 18, 19]. Currently, in Vietnam, according to our research, there is still no research on the application of tomography to determine the hollow capacity inside the trunk. Therefore, our work is the first time in Vietnam focusing on applying geophysical methods to tree investigation.

In the application of geoelectrical methods to image subsurface, the electrodes are usually located above the ground (Fig. 1a). This is related to the boundary conditions between the ground and the air. For the survey to investigate inside the trunk, the electrodes are arranged around the tree trunk (Fig. 1b). In this case, the solution approach of the problem is different from the case of probing underground objects. Therefore, it is necessary to have studies to change the transformation processes of measurement and data

processing to suit the task of tree investigation.

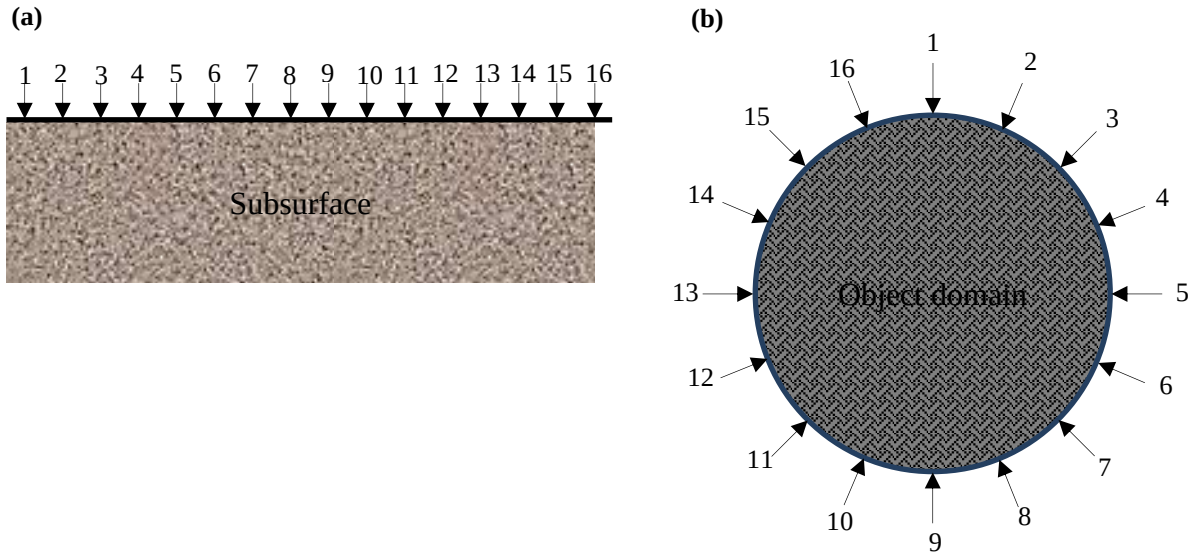

Fig. 1. Electrode's configuration. Conventional configuration of array in geophysical survey on the surface (a), the configuration around boundaries (b).

2. Theory background

In the Electrical impedance tomography (EIT) method, we inject known amounts of current into a medium that produces current fluxes and induce potentials. We measure the potential electrical field at points on the boundary of the medium (Fig. 1). The current fluxes and potential at the object boundary are influenced by the object impedance. For example, the current conduction within a homogeneous domain (Fig. 2a) differs from that in an inhomogeneous domain (Fig. 2b). As a result, the voltage profile of the homogenous object will be different from the domain with inhomogeneity. It is similar at the boundary; potential profiles will depend on the domain impedance distribution. In other words, we can obtain the information of the impedance distribution of the object domain from the potential boundary data. Also, it is possible to construct a map of the conductivity or resistivity of the region of the object domain.

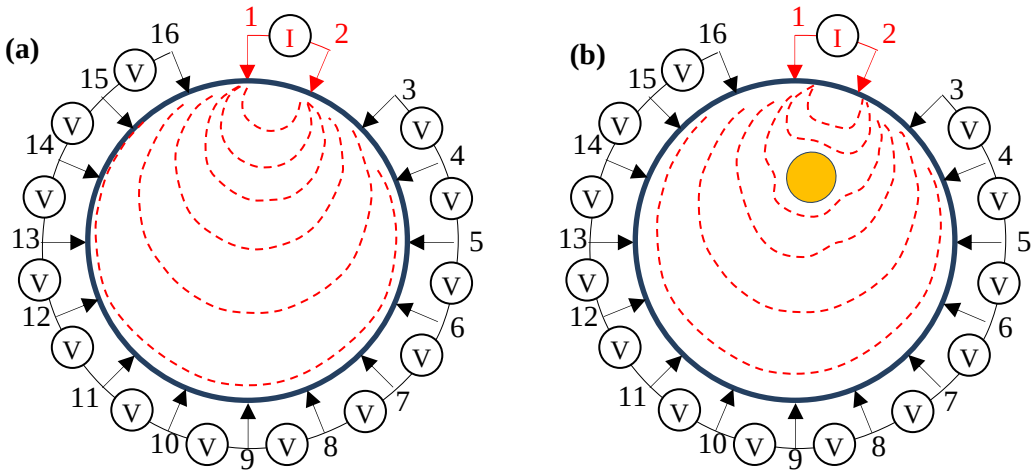

Fig. 2. Variation in boundary data profiles for a homogeneous domain (a) and an inhomogeneous domain (b). The red dash lines show electric current.

a. The governing equations inside the object domain

In an inhomogeneous medium, Maxwell's equations are following:

$$\nabla \times E = -\frac{\partial B}{\partial t}, \quad (1a)$$

$$\nabla \times H = J + \frac{\partial D}{\partial t}, \quad (1b)$$

where E and H is electric and magnetic fields, respectively, B *is* magnetic induction, D *is* electric displacement and J electric current density. Moreover, in linear isotropic medium the following relations are valid:

$$D = \varepsilon E, \quad (2a)$$
$$B = \mu H, \quad (2b)$$
$$J = \sigma E, \quad (2c)$$

where ε and μ are electrical and magnetic permittivity, respectively, and σ is the conductivity of the medium. Assuming that the injected currents are time-harmonic with frequency ω, the electric and magnetic fields are of the form (Eqs. 3a and 3b).

$$E = E_0 e^{i\omega t}, \quad (3a)$$
$$B = B_0 e^{i\omega t}. \quad (3b)$$

Using the relations (Eqs. 2a, 2b and 2c), we can rewrite electric and magnetic fields (eqs. 1a and 1b) as follow:

$$\nabla \times E = -i\omega\mu H, \quad (4a)$$
$$\nabla \times H = J + i\omega\varepsilon E. \quad (4b)$$

The quasi-static approximation usually employed in EIT is to assume $\omega\mu H$ is negligible, thus from equation (4a) we have $\nabla \times E = 0$ and hence

$$E = -\nabla\emptyset, \quad (5)$$

where $\emptyset$ is scalar potential.

In EIT, the total current is $J = J_0 + J_S$ where J_s is source current, it is typically zero at frequency ω, and ohmic current $J_0 = \sigma E$. We assume that $\sigma \gg i\omega\varepsilon$, the equation (4b) can be rewritten:

$$\nabla \times H = \sigma E. \quad (6)$$

Substituting E in equation 5 in equation 6 and taking the divergence on both sides, we achieve Laplace's equation (6).

$$\nabla \cdot (\sigma \nabla\emptyset) = 0. \quad (7)$$

The current density on the boundary is

$$j = -J_S \cdot \boldsymbol{n} = \sigma\nabla\emptyset \cdot \boldsymbol{n}, \quad (8)$$

where $\boldsymbol{n}$ is the outward unit normal to boundary $\partial\Omega$, where j is the negative normal component of the injected current density J_S. Laplace's equation (7) and the boundary conditions (8) is used to build a mathematical model of the EIT method [20].

b. Modeling and inversion

In this work, we use a model of 16 electrodes (Fig. 3). This is the best number to reconstruct the lungs image [21]. The electric resistivity of the wood varies with tree species (Tab. 1), and it is mostly influenced by the water content, chemical elements, which change according to the status of wood and cell structure. Reaction wood does have different resistivity compared to “normal wood”. The models (Fig. 3) represent three scenarios of the trunk: (1) normal status the trunk is homogeneous (Fig. 3a); there is an area inside the trunk, the wood is decayed and contains saline water causing high conductive abnormal (Fig. 3b); and there is an area inside the trunk, the wood is decayed and contains air causing low conductive anomaly (Fig.

3c). In this work, we use an open-source software suite for image reconstruction in electrical impedance tomography and diffuse optical tomography EIDORS [18] for forward and inversion of the data.

Fig. 3. Model of the tree trunk with homogeneous impedance distribution (a), there is a conductive

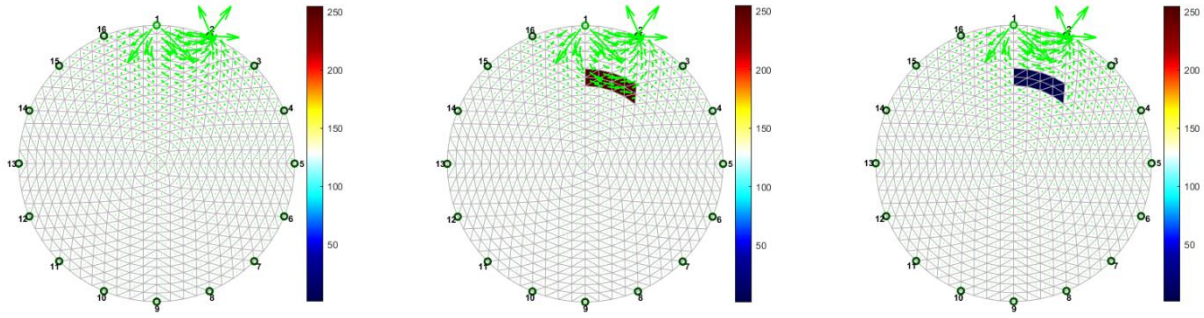

(a) (b) (c)

abnormal area (b), and there is a resistive abnormal area (c). Color bars show relative conductivity of the domain, and dark blue represents more conductive, dark red illustrates more conductive domain. The green arrows show electric current flow; longer arrows represent larger currents.

Tab. 1. Electrical resistivity (ER) parameters (mean ± SE, minimum and maximum) for tomograms performed at different temperatures (Temp.). For each tree, the stem diameter (Diam.) at measurement height is given [16].

Tree species	ERmean (Ωm)	ERmax (Ωm)	ERmin (Ωm)
B. pendula	136.34 ± 1.36	755.33	8.66
F. sylvatica	265.08 ± 4.60	1007.48	8.07
P. nigra	80.22 ± 0.94	177.82	8.97
L. decidua	276.53 ± 5.18	1279.42	22.04
P. abies	314.89 ± 5.19	975.58	25.65

The synthetic data generated from the models in Fig. ***3***b and c are added 5% Gaussian noise and running inversion process using an approach of Adler and Guardo [22]. The results are shown in Fig. ***4***. The constructed images show that we can well define the location of decay areas for both models; however, the images of the inverted model are larger than the true areas of the models. Further works of the inversion process are needed to improve the reconstructed images in the future.

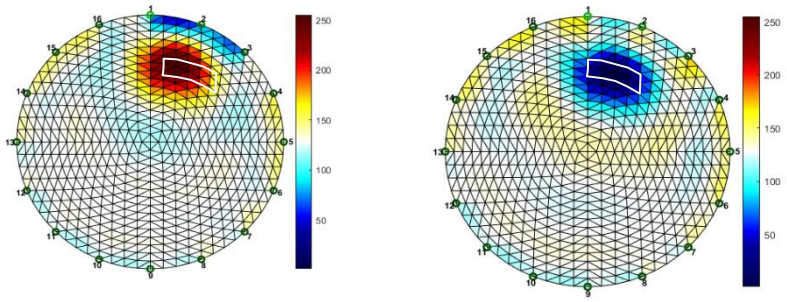

(a) **(b)**

Fig. 4. Inversion results of synthetic data generated by using the conductive model (Fig. 3a) (a) and the resistive model (Fig. 3b) (b). The white polygons mark the true models.

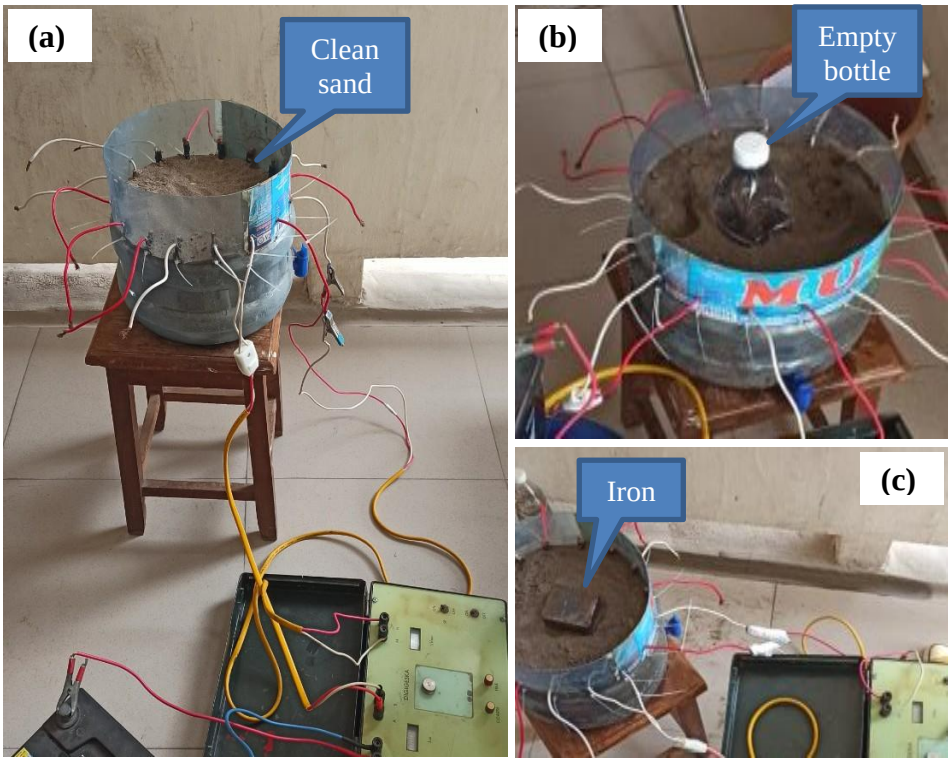

Fig. 5. Experiment models. We use a cylindrical plastic container of sand as the homogeneous model (a), an empty bottle is buried in the center of the cylindrical plastic container represent resistive model (b), and a cubic iron is a conductive model (c).

3. Laboratory experiment

a. Designing experiment models

We use a cylindrical plastic container bottle to make an experiment model (Fig. 5). Copper electrodes are fixed around this cylindrical plastic container. Inside the container, we fill it with moist clean sand to build the homogenous model (Fig. 5a). In one case, we want to build a model with a high resistivity anomaly region, and we use an empty plastic bottle placed in the center of the model (Fig. 5b). In the opposite case, if we want to have a model with a good conductive region, we use iron in the middle of the model (Fig. 5c).

We use a Digigeska electrical instrument made by Geophysical Division, Vietnam, to measure. This is a conventional electrical instrument for four electrodes measurement, a pair of current electrodes, and a pair of potential electrodes. We have a total of 16 electrodes. We have to manually change electrodes at each measurement. First, the current is applied through electrodes 1 and 2 (Fig. 2). The voltage is measured successively with potential electrode pairs 3-4, 4-5, . . . 15-16. Thus, we get 13 voltage measurements. And then, we change the pair of current electrodes to 2 and 3 and measure the voltage of the remaining 13 pairs of electrodes. We continue to change the current electrodes to 16. In total, we obtained 208 measurements.

The data is put in the inversion process, and the results are shown in Fig. 6. We can see that reconstructed images illustrate the models. In the case of the homogeneous model, the container is filled with moist clean sand only. The relative conductivity of the model (Fig. 6b) varies around zero. In the case of the resistive model (Fig. 6a) and conductive model (Fig. 6c), the negative and positive abnormal show the location of the empty bottle and cubic iron, respectively. However, the constructed images do not show the locations and areas of the two objects perfectly, and we can see some artifacts. These may be caused by the highly noisy measured data and the inversion with smooth constraints.

b. Testing on the real wood in the laboratory

We found a solid trunk, which can be seen as a healthy trunk, free from pests and diseases (Fig. 7a). First, we carried out the measurement as described in the experimental model section. We then used a

hollow chisel in the middle to make a model of the hollow trunk (Fig. 7b). Finally, we filled the hollow with hydrated sand to simulate a hollow tree trunk containing water (Fig. 7c). The measurement process is similar to the first case.

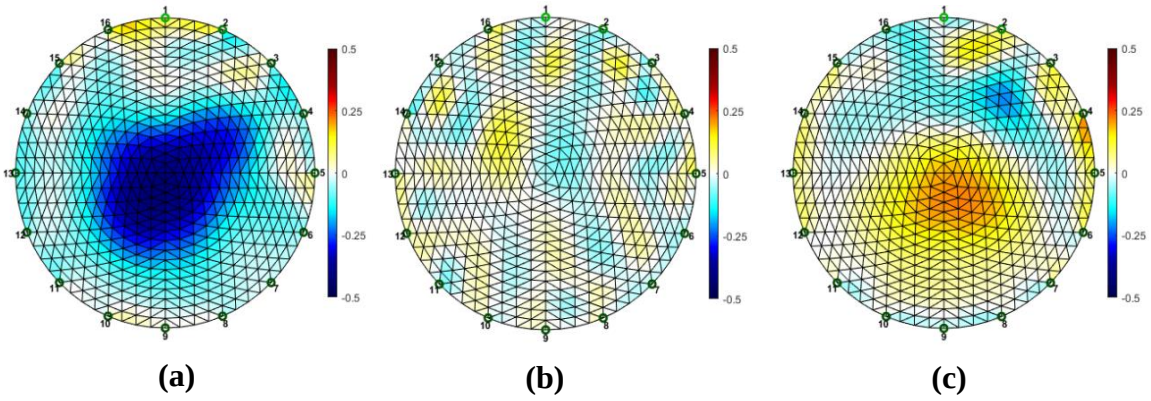

Fig. 6. The inversion results of the experiment data. The constructed image of the resistive model (a), homogeneous model (b), and conductive model (c). The color bars show the relative conductivity of the models; blue and red represent resistive and conductive mediums, respectively.

The inversion process is also applied as similar to the experiment models. The results are shown in Fig. 8. We can see that reconstructed images illustrate the wood models. In the case of the homogeneous model (healthy trunk), the relative conductivity of the model (Fig. 8b) varies around zero. In the case of the resistive model (Fig. 8a) and conductive model (Fig. 8c), the negative and positive anomalies show the locations of the empty hollow and hydrated sand, respectively. The issue is like the container models above; the constructed images do not show areas of the two abnormal areas perfectly. These may be caused by the highly noisy measured data and the inversion with smooth constraints.

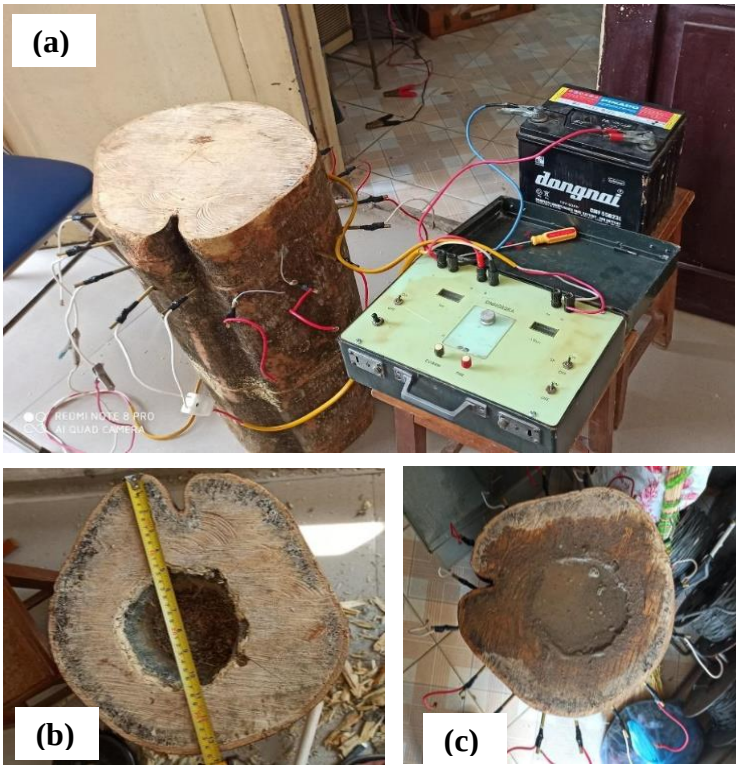

Fig. 7. The wooden models. We have a homogeneous trunk (a), we hollowed out the trunk of the tree to make the model of a hollow trunk containing air (b) and finally we put sand and water inside the hole to make the conductive model of the trunk.

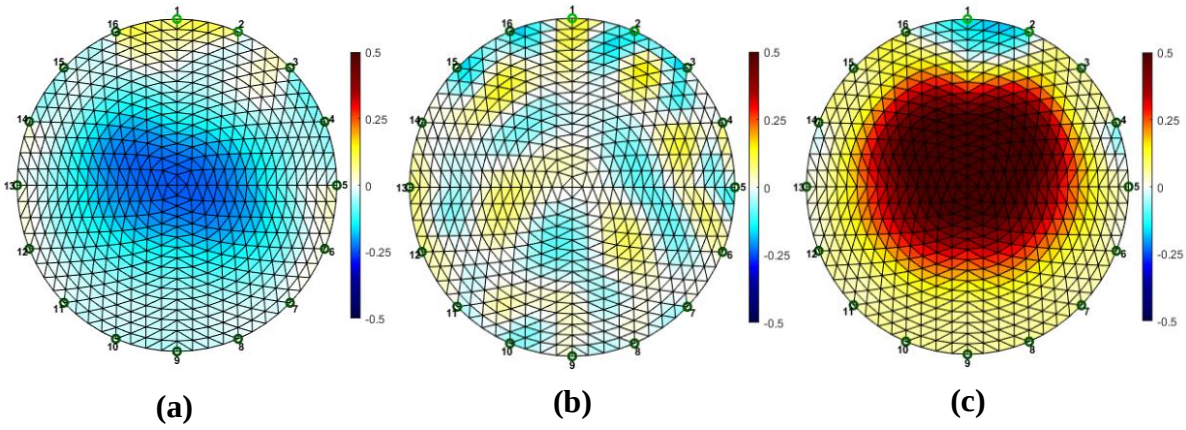

Fig. 8. The inversion results of the experiment data. The constructed image of the resistive model (a), homogeneous model (b) and conductive model (c). The color bars show relative conductivity of the models, blue and red represent resistive and conductive medium, respectively.

4. Real data

The data were measured on two perennial mango trees, planted next to each other and about the same age, about 350 years old. One tree has broken branches due to hollow trunks (Fig. 9). The question is when the remaining tree will break in the future.

The measurement and inversion approaches are similar in the laboratory. We use 16 electrodes and measure the pattern in succession between two electrodes next to each other (Fig. 10a). The constructed image (Fig. 10b) clearly shows the low conductivity part related to the hollow part of the trunk. We made similar measurements on the remainder tree (Fig. 11a) and the results also indicated that there is a hollow in the middle part of the trunk (Fig. 11b).

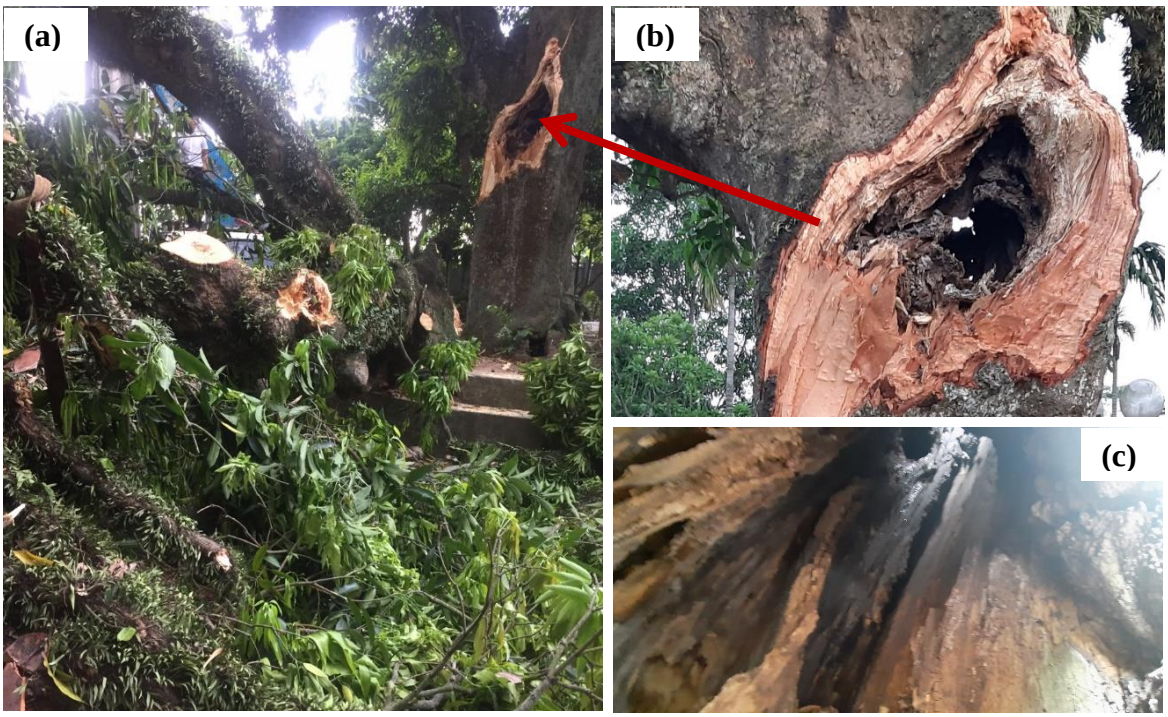

Fig. 9. The hollow tree is the cause of the broken branches (a). Zoom in on the broken branch due to the hollow inside (b). Image of the hollow inside the tree (c).

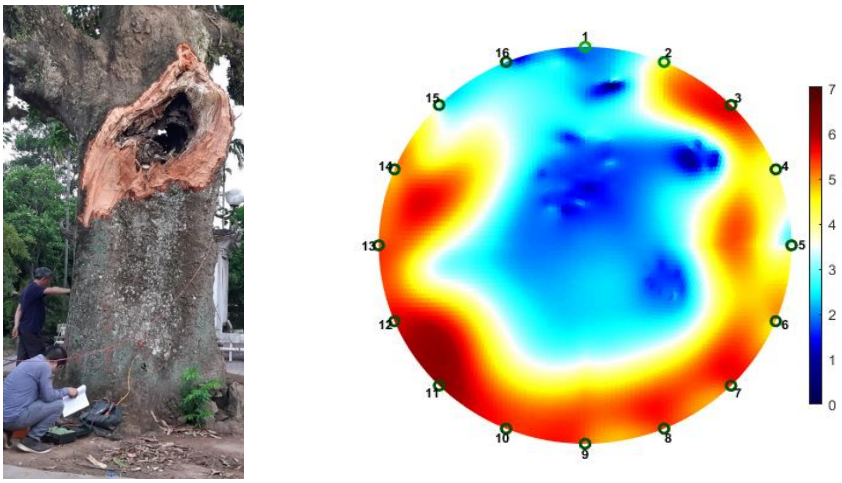

(a) **(b)**

Fig. 10. Measurement of the broken tree (a). The inversion image shows clearly resistive area (blue color) that illustrates the hollow inside the tree (b). The color bar shows relative conductivity of the models. Blue and red represent resistive and conductive media, respectively.

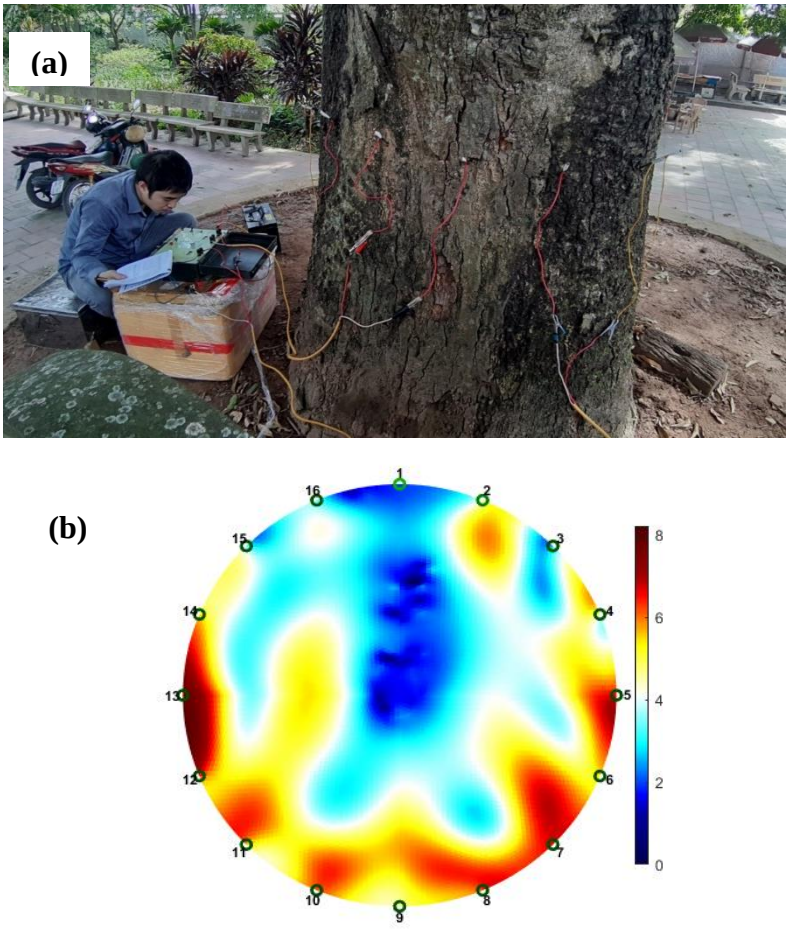

Fig. 11. Measurement of the tree is located near the broken tree (a). The inversion image clearly shows the resistive area (blue color) that may illustrate the hollow inside the tree (b). The color bar shows the relative conductivity of the models; blue and red represent resistive and conductive mediums, respectively.

5. Conclusion

We present the application of the electrical impedance tomography (EIT) method to investigate the inside of trees in Vietnam. The biggest advantage of this method is the non-destructive sample, i.e., the method can be applied to investigate the trees with no damage to them. We have built theoretical models and laboratory experiments and then test in real cases. Our preliminary results demonstrate that the EIT method is robust to investigate the trees. However, the results are not yet perfect, and we believe that further research can improve the results. In the future, a better instrument to acquire data and an improved inversion process to construct the tree image can enhance the robustness of the EIT method.

6. Acknowledgments

This paper is completed as a result of the project funded by the Hanoi University of Mining and Geology, code T21-22. We would like to thank the geophysics students, Pham Van Kien, Nguyen Huu Thang, Tran Phung Trung Hien, Tran Dang Tuan, and Nguyen Tuan Thanh, who assisted us in building experimental models and conducting measurements. We sincerely thank Mr. Nguyen Van Loi, Institute of Ecology and Works Protection, for supporting us in collecting the real data. We would like to thank all the authors of the EIDORS Source code that is used in this work http://www.sce.carleton.ca/faculty/adler/eidors/programming/programming.shtml.

The paper was presented during the 6th VIET - POL International Conference on Scientific-Research Cooperation between Vietnam and Poland, 10-14.11.2021, HUMG, Hanoi, Vietnam.

7. References

1. http://www.vacne.org.vn/4-018-old-trees-across-the-country-have-been-recognized-as-vietnamese-heritage-trees/e3699.html, 08/07/2021.
2. Loke, M.H., J.E. Chambers, D.F. Rucker, O. Kuras, and P.B. Wilkinson, 2013. Recent developments in the direct-current geoelectrical imaging method. Journal of Applied Geophysics, 95: 135-156.
3. Pidlisecky, A., E. Haber, and R. Knight, 2007. RESINVM3D: A 3D resistivity inversion package. Geophysics, 72(2): H1-H10.
4. Kieu, T.D., 2020. Inversion of multiple data sets acquired by different array configuration of geoelectrical resistivity method (in Vietnamese) Journal of Mining and Earth Sciences, 61(1): 52-60.
5. Kemna, A., J. Vanderborght, B. Kulessa, and H. Vereecken, 2002. Imaging and characterisation of subsurface solute transport using electrical resistivity tomography (ERT) and equivalent transport models. Journal of Hydrology, 267(3): 125-146.
6. Chambers, J.E., O. Kuras, P.I. Meldrum, R.D. Ogilvy, and J. Hollands, 2006. Electrical resistivity tomography applied to geologic, hydrogeologic, and engineering investigations at a former waste-disposal site. Geophysics, 71(6): B231-B239.
7. Dat, P.N., P.N. Kien, B.V. Thom, L.H. Phong, and D.T. Ninh, 2018. Determining the thickness of the weathering layer overlying the basalt in Cu Mga - Dak Lak area by 2D resistivity imaging, Journal of Mining and Earth Sciences, 59(6): 1-10.
8. Perrone, A., V. Lapenna, and S. Piscitelli, 2014. Electrical resistivity tomography technique for landslide investigation: A review. Earth-Science Reviews, 135: 65-82.
9. Samouëlian, A., I. Cousin, A. Tabbagh, A. Bruand, and G. Richard, 2005. Electrical resistivity survey in soil science: a review. Soil and Tillage Research, 83(2): 173-193.
10. Bera, T.K., 2014. Bioelectrical Impedance Methods for Noninvasive Health Monitoring: A Review. Journal of medical engineering, 381251.
11. Luo, Y., P. Abiri, S. Zhang, C.-C. Chang, A.H. Kaboodrangi, R. Li, A.K. Sahib, A. Bui, R. Kumar, M. Woo, Z. Li, R.R.S. Packard, Y.-C. Tai, and T.K. Hsiai, 2018. Non-Invasive Electrical Impedance Tomography for Multi-Scale Detection of Liver Fat Content. Theranostics, 8(6): 1636-1647.
12. Sambuelli, L., L.V. Socco, and A. Godio, 2003. Ultrasonic, electric and radar measurements for living trees assessment. Bollettino di Geofisica Teorica ed Applicata, 44: 253-279.

13. Attia al Hagrey, S., 2007. Geophysical imaging of root-zone, trunk, and moisture heterogeneity. Journal of Experimental Botany, 58(4): 839-854.
14. Jayawickreme, D.H., E.G. Jobbágy, and R.B. Jackson, 2014. Geophysical subsurface imaging for ecological applications, 201(4): 1170-1175.
15. Corona-Lopez, D.D.J., S. Sommer, S.A. Rolfe, F. Podd, and B.D. Grieve, 2019. Electrical impedance tomography as a tool for phenotyping plant roots. Plant Methods, 15(1): p. 49.
16. Cimpoiaşu, M.O., O. Kuras, T. Pridmore, and S.J. Mooney, 2020. Potential of geoelectrical methods to monitor root zone processes and structure: A review. Geoderma, 365: 114-232.
17. Malmivuo, J. and R. Plonsey, 1995. Bioelectromagnetism. 26. Impedance Tomography, 420-427.
18. Ehosioke, S., F. Nguyen, S. Rao, T. Kremer, E. Placencia-Gomez, J.A. Huisman, A. Kemna, M. Javaux, and S. Garré, 2020. Sensing the electrical properties of roots: A review, 19(1): e20082.
19. Ganthaler, A., J. Sailer, A. Bär, A. Losso, and S. Mayr, 2019. Noninvasive Analysis of Tree Stems by Electrical Resistivity Tomography: Unraveling the Effects of Temperature, Water Status, and Electrode Installation. Frontiers in plant science, 10: 1455-1455.
20. Polydorides, N., 2002. Image reconstruction algorithms for soft-field tomography, in Electrical Engineering and Electronics. University of Manchester : UMIST: University of Manchester : UMIST. p. 262.
21. Schullcke, B., S. Krueger-Ziolek, B. Gong, and K. Moeller, 2016. Effect of the number of electrodes on the reconstructed lung shape in electrical impedance tomography. Current Directions in Biomedical Engineering, 2.
22. Adler, A. and R. Guardo, 1996. Electrical impedance tomography: regularized imaging and contrast detection. IEEE Transactions on Medical Imaging, 15(2): 170-179.